

AN IMPROVED LIMITER FOR MULTIDIMENSIONAL FLUX–CORRECTED TRANSPORT

C. Richard DeVore

Laboratory for Computational Physics and Fluid Dynamics

Naval Research Laboratory

Washington, DC 20375–5344

ABSTRACT

An improved prescription is given for limiting (‘correcting’) the high-order fluxes in multidimensional, flux–corrected transport (FCT) algorithms. These fluxes are designed to reduce the numerical error in positive-definite, monotone solutions to the hydrodynamics equations. The role of the limiter is to ensure that the desirable positivity and monotonicity properties of the low-order solutions are not lost in the quest to minimize the numerical error. It is shown that Zalesak’s (1979) formulation of a limiter for multidimensional FCT preserves positivity but not monotonicity. The introduction of a prelimiting step into his prescription, based on the original positive and monotone limiter of Boris and Book (1973), is proposed and is shown to improve significantly the performance of multidimensional FCT algorithms.

CONTENTS

1. Introduction	1
2. Generalized Continuity Equations and FCT	2
3. Boris and Book's Limiter	4
4. Zalesak's Limiter	5
5. A Monotone Multidimensional Limiter	8
6. Examples	9
7. Discussion	17
Acknowledgements	18
References	18

AN IMPROVED LIMITER FOR MULTIDIMENSIONAL FLUX-CORRECTED TRANSPORT

1. INTRODUCTION

Flux-corrected transport, or FCT (Boris & Book 1973; Book, Boris & Hain 1975; Boris & Book 1976a, 1976b; Zalesak 1979; DeVore 1989, 1991; Boris *et al.* 1993), was developed, and has been used extensively by many investigators, to accurately solve the conservation equations of Eulerian hydrodynamics without violating the positivity of mass and energy, particularly in the vicinity of shock waves and other discontinuities. This is achieved by adding to the equations a strong numerical diffusion, which guarantees the positivity of the solution, followed by a compensating antidiffusion, which reduces the numerical error. The crux of the FCT method lies in limiting ('correcting') these antidiffusive fluxes before they are applied, so that no unphysical extrema are created in the solution. The goal of the flux-correction procedure is to provide as accurate a solution to the original equation as is consistent with maintaining positivity and monotonicity everywhere.

The original limiter of Boris and Book (1973) applies several tests to the sign and magnitude of the antidiffusive flux at each cell boundary, taking into account the profile of the transported quantity (*e.g.*, the mass or energy density) in the neighborhood of that boundary. In one spatial dimension, these tests can be condensed into a single, relatively simple formula for the corrected antidiffusive fluxes, which then are guaranteed to preserve the positivity and monotonicity of the transported variable. For certain multidimensional hydrodynamics applications, this limiter and its underlying integration scheme can be employed in a serial fashion to each of the coordinate directions in turn, using Strang operator splitting (Oran & Boris 1987).

Certain classes of problems, however, call for a fully multidimensional approach. These include incompressible or nearly incompressible flows, flows with a high degree of symmetry, and magnetohydrodynamic (MHD) systems. Zalesak (1979) analyzed Boris and Book's one-dimensional limiter, identified the tests inherent in it, and showed why a reformulation was needed to extend the FCT approach to multidimensional situations. He provided such a formulation, showed that his new limiter could be made equivalent to the original, and then illustrated it with several one- and two-dimensional examples.

Zalesak's multidimensional limiter has been used by the author in both hydrodynamic and MHD (DeVore 1989; DeVore 1991) FCT algorithms in recent years, with applications

to shock and detonation waves (Oran & DeVore 1994), shear flows and jets (Grinstein 1995; Grinstein & DeVore 1996), and arcades of plasma and magnetic field in the solar atmosphere (Karpen, Antiochos & DeVore 1990, 1991, 1994, 1996; Karpen *et al.* 1998; Antiochos, DeVore & Klimchuk 1999; Antiochos & DeVore 1999a, 1999b), among others. Those experiences have shown that the limiter is positivity- but not monotonicity-preserving, yielding solutions with numerical ripples of significant amplitude in many cases. The purpose of this paper is to show why this occurs and to propose a modification of Zalesak’s limiter which contributes greatly towards preserving monotone profiles. The recommended modification is the addition of a prelimiting step based on Boris and Book’s original limiter, which is both positive and monotone. Zalesak in fact suggested this approach in passing in his earlier work, but did not explore its ramifications and did not promote its regular use. We do both in the remainder of this paper.

2. GENERALIZED CONTINUITY EQUATIONS AND FCT

The conservation equations of Eulerian hydrodynamics take the general form

$$\frac{\partial \rho}{\partial t} + \nabla \cdot (\rho \mathbf{v}) = S, \tag{1}$$

where ρ is a fluid variable (mass, momentum, or energy density) being time-advanced, \mathbf{v} is the fluid velocity, and S is a source term. In a finite-volume, Eulerian representation of Eq. (1), the mass, momentum, or energy enclosed in each computational cell evolves due to sources and due to the convective fluxes through the faces of that cell. Each such flux defined on an interior face of the domain increments the amount of mass in the cell which the flux is entering, and decrements it by an equal amount in the cell which it is exiting. This leaves the total mass of the system unchanged, *i.e.*, the integration scheme is conservative.

Any discrete representation of the convective fluxes in Eq. (1) introduces numerical errors into the solution for ρ . Indeed, a central difference representation of the fluxes – wherein the face value of ρ is just the average of the cell values ahead of and behind the face – produces an absolutely unstable solution for any finite velocity \mathbf{v} . These errors can be reduced by introducing additional numerical terms into Eq. (1), which also are defined in terms of fluxes so that the integration scheme remains conservative. In particular, the addition of a smoothing diffusion term of sufficient amplitude stabilizes the convective terms and also imposes one other important physical constraint on the solution: positivity.

This ensures that the evolution of a positive-definite initial profile ρ^o does not lead to unphysically negative densities as a consequence of convection alone.

The result of this integration procedure is a provisional solution ρ^ℓ which is positive except where the sources S are negative and sufficiently large to produce a reversal in sign, and is monotone except where either convection or sources, or both together, act to produce extrema.

The strong numerical diffusion required to guarantee the positivity of the solution ρ^ℓ is too large to be satisfactory for most hydrodynamics applications. In regions where the density is slowly varying, it is advantageous to apply antidiffusive fluxes which compensate for the previously applied diffusion and yield a high-order accurate solution ρ^h to Eq. (1). Unfortunately, near discontinuities this procedure is perilous, as the attempt to fit a high-order solution can produce a highly oscillatory solution. Both the positivity and monotonicity properties of the provisional solution can be lost in this effort.

With flux-corrected transport (FCT), Boris and Book (1973) resolved the conflicting demands for a positive, monotone solution such as ρ^ℓ on the one hand, and for an accurate, nondiffusive solution such as ρ^h on the other. Their approach is to limit the antidiffusive fluxes which change ρ^ℓ into ρ^h so that *no new extrema are created, nor are any existing extrema enhanced* by the application of the corrected fluxes. The rule which they implemented to achieve this objective will be considered momentarily. The FCT prescription for solving generalized continuity equations such as Eq. (1) can be summarized as follows:

1. Convect ρ .
2. Numerically diffuse ρ sufficiently to ensure that the result is positive everywhere, if the initial profile ρ^o is positive.
3. Add sources S to obtain the low-order, provisional solution ρ^ℓ .
4. Compute numerical antidiffusive fluxes which would convert ρ^ℓ to a high-order accurate solution ρ^h .
5. Limit these antidiffusive fluxes so that no new extrema will be created and no existing extrema will be enhanced.
6. Apply the corrected fluxes to ρ^ℓ to obtain the desired solution ρ^n .

The combination of the positive, monotone solution from steps 1 and 2 with the restrictive action of the flux limiter in step 5 ensures that the result ρ^n also will be positive and

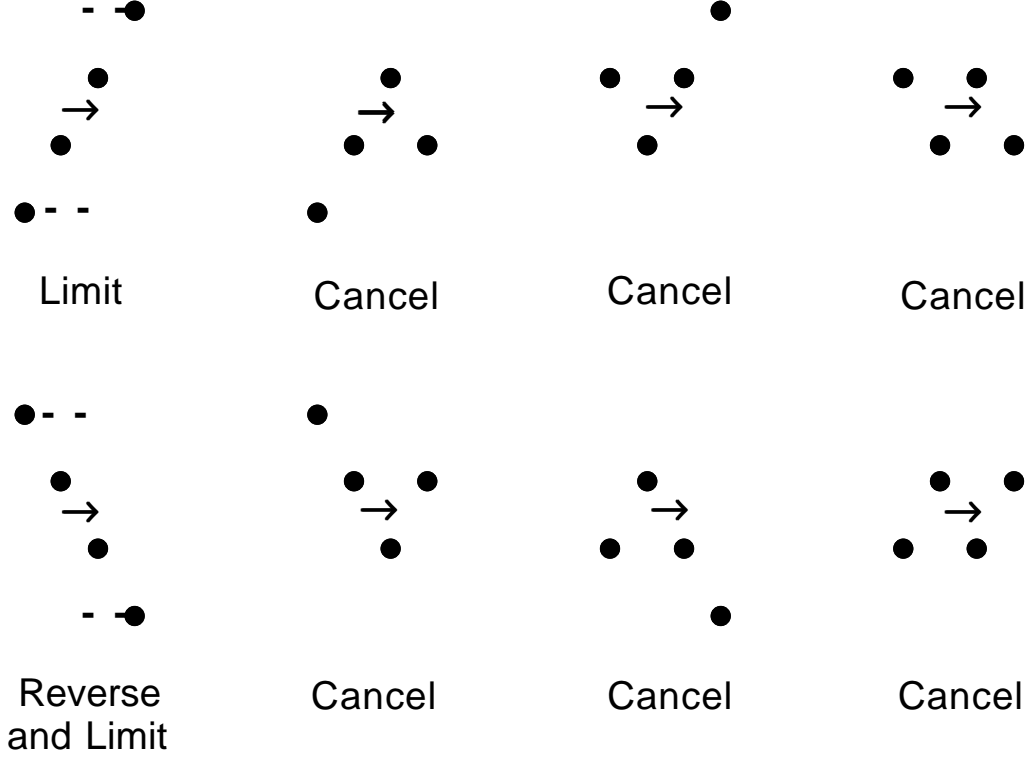


Fig. 1. The action of Boris and Book’s flux limiter for one-dimensional FCT is indicated for the eight possible configurations of four grid points (\bullet) surrounding an antidiffusive flux (\rightarrow) here shown directed to the right. The dashed lines in the leftmost panel indicate the maximum excursion allowed the two middle points when the corrected flux is applied, so that no new extrema are created. In the middle and rightmost panels, the flux is cancelled to avoid enhancing existing extrema. On the bottom row, the flux is reversed in direction so that it acts to steepen the profile.

monotone except where the physics of convection and sources together produce extrema. Spurious numerical extrema are avoided.

3. BORIS AND BOOK’S LIMITER

In their original paper on FCT, Boris and Book (1973) provided a rule for limiting the antidiffusive fluxes when solving generalized continuity equations in one spatial dimension. Given the provisional profile ρ_i^ℓ , the cell volumes V_i , and the raw antidiffusive fluxes $F_{i+1/2}^a$ defined on the cell faces, where i is a cell index, the rule is

$$F_{i+1/2}^c = \sigma_{i+1/2} \max \left[0, \min \left(\left| F_{i+1/2}^a \right|, \sigma_{i+1/2} V_i \Delta \rho_{i-1/2}^\ell, \sigma_{i+1/2} V_{i+1} \Delta \rho_{i+3/2}^\ell \right) \right]. \quad (2)$$

Here $F_{i+1/2}^c$ is the corrected (positivity- and monotonicity-preserving) antidiffusive flux, $\Delta\rho^\ell$ is a density difference,

$$\Delta\rho_{i+1/2}^\ell \equiv \rho_{i+1}^\ell - \rho_i^\ell, \quad (3)$$

and σ is its sign,

$$\sigma_{i+1/2} \equiv \text{sign } \Delta\rho_{i+1/2}^\ell, \quad (4)$$

with $|\sigma| = 1$.

This flux limiter has the following consequences:

- If the ρ^ℓ profile is *not* monotone between cells $i-1$ and $i+2$, which means that at last one of ρ_i^ℓ and ρ_{i+1}^ℓ is a local extremum and $\Delta\rho^\ell$ changes sign, then the flux is cancelled.
- If the ρ^ℓ profile *is* monotone over that range, then the amplitude of the flux is limited to the smallest of its original magnitude and the two mass changes sufficient to flatten the profile ahead of and behind the interface.
- If the raw antidiffusive flux is directed down the gradient of ρ^ℓ , so that it smooths rather than steepens the profile, then the sign of the flux is reversed (it is given the sign of $\Delta\rho^\ell$) and the amplitude is limited according to the above criteria.

These consequences are displayed schematically in Fig. 1.

A consideration of the flux limiter (2) and its actions in the various scenarios sketched in Fig. 1 shows that its stated goal is met: *no new extrema are created, nor are any existing extrema enhanced* as a result of the antidiffusion stage of the algorithm. The former is ensured by the amplitude limitation inherent in the flux-correction formula; the latter by the complete cancellation where the density difference reverses sign.

4. ZALESK'S LIMITER

In his analysis of the flux limiting formula (2) to derive an extension of it to two or more spatial dimensions, Zalesak (1979) noted the remarkable fact that each flux is limited independently; there is no consideration of the effect of multiple fluxes acting in concert. Upon reflection, this is to be expected in one dimension because both fluxes enter or leave a cell only if that cell is a local maximum or minimum, respectively. In either instance, both fluxes must be cancelled to avoid accentuating the already existing extremum. This cancellation is already built into the flux limiter, however, so knowledge about the sign and magnitude of neighboring fluxes is not required in (2).

The situation is different in two or more dimensions, where multiple fluxes may enter or leave a cell without that cell being a local extremum. As a result, the flux limiter must take into account the consequences of fluxes acting in concert. Zalesak reformulated the one-dimensional flux limiter in a way that preserves the desirable properties of Boris and Book's limiter, but also generalizes immediately to multidimensional problems. His procedure is as follows:

- A. Establish allowed extrema ρ^{\min} and ρ^{\max} in each cell; for consistency with Boris and Book, set

$$\begin{aligned}\rho_i^{\min} &= \min(\rho_{i-1}^\ell, \rho_i^\ell, \rho_{i+1}^\ell), \\ \rho_i^{\max} &= \max(\rho_{i-1}^\ell, \rho_i^\ell, \rho_{i+1}^\ell).\end{aligned}\tag{5}$$

- B. Reverse the sign of any antidiffusive flux that is directed down the gradient of ρ^ℓ , *viz.*,

$$F_{i+1/2}^{a'} = \sigma_{i+1/2} \left| F_{i+1/2}^a \right|.\tag{6}$$

- C. Compute the total incoming and outgoing antidiffusive fluxes F^{in} and F^{out} in each cell,

$$\begin{aligned}F_i^{\text{in}} &= \max(F_{i-1/2}^{a'}, 0) - \min(F_{i+1/2}^{a'}, 0), \\ F_i^{\text{out}} &= \max(F_{i+1/2}^{a'}, 0) - \min(F_{i-1/2}^{a'}, 0).\end{aligned}\tag{7}$$

- D. Determine the fractions of the incoming and outgoing fluxes that can be applied to each cell,

$$\begin{aligned}f_i^{\text{in}} &= (\rho_i^{\max} - \rho_i^\ell) V_i / F_i^{\text{in}}, \\ f_i^{\text{out}} &= (\rho_i^\ell - \rho_i^{\min}) V_i / F_i^{\text{out}}.\end{aligned}\tag{8}$$

- E. Limit each antidiffusive flux so that it creates neither an undershoot in the cell it is leaving nor an overshoot in the cell it is entering,

$$F_{i+1/2}^c = F_{i+1/2}^{a'} \times \begin{cases} \min(f_i^{\text{out}}, f_{i+1}^{\text{in}}, 1), & \text{if } F_{i+1/2}^{a'} \geq 0; \\ \min(f_i^{\text{in}}, f_{i+1}^{\text{out}}, 1), & \text{otherwise.} \end{cases}\tag{9}$$

Zalesak's step B as given in his paper is different from the one above, and his is not fully consistent with the original limiter. The discrepancy is that he used the sign of the antidiffusive flux F^a , rather than the sign of the density difference $\Delta\rho^\ell$, for σ in Eq. (2). As he noted, this adjustment is relatively rarely applied in any case – the majority of raw antidiffusive fluxes act to steepen the gradient – but it does serve to suppress the generation of numerical ripples. Also, Zalesak pointed out and showed through several

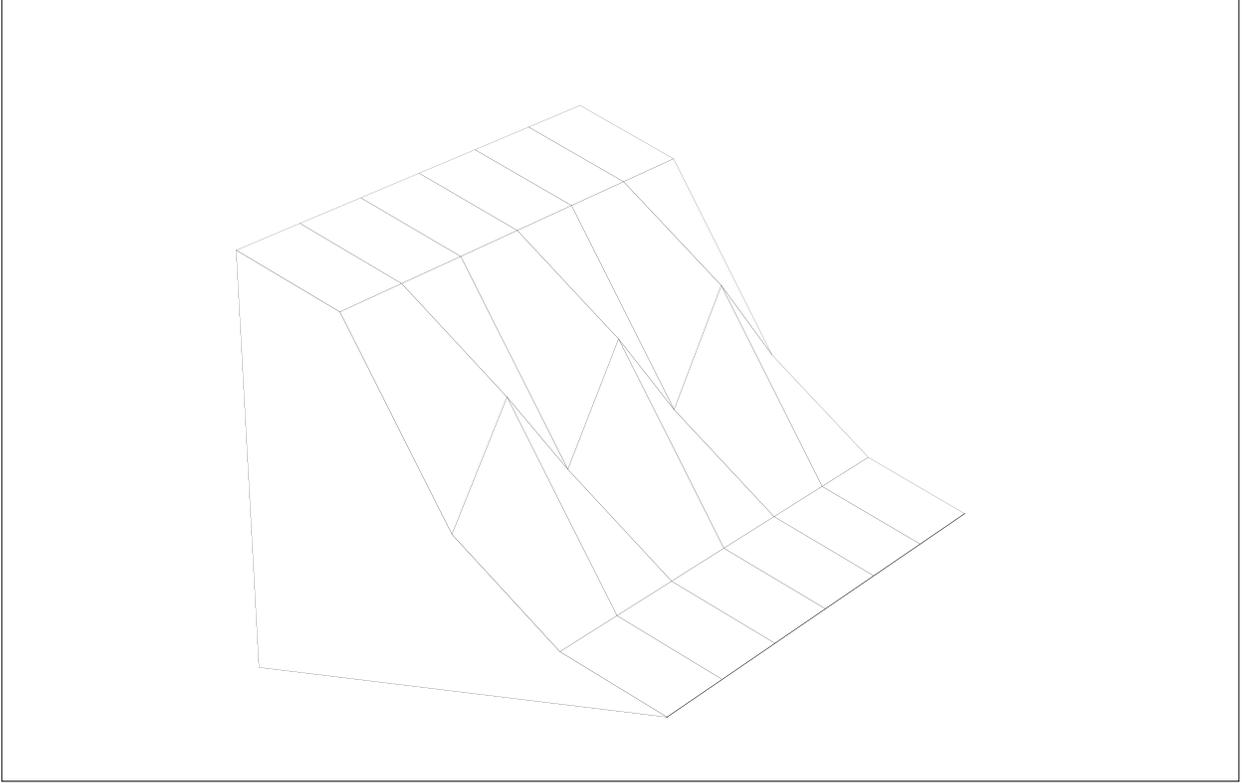


Fig. 2. A quasi-one-dimensional discontinuity propagating in 2D is shown as a surface plot. Each junction of lines represents a grid point (cell center) where the density ρ^ℓ is defined. Transverse to the principal discontinuity, which is oriented left to right, is a ripple in the solution. Zalesak's flux limiter in 2D will allow this ripple to be created and amplified, so long as the extrema along the ripple lie within those of the principal discontinuity transverse to it.

examples how the limiter can be made more flexible by generalizing the formulae of step A for the allowed extrema.

The flux limiter as reformulated by Zalesak has the following consequences:

- It can be made identical to Boris and Book's limiter in one spatial dimension.
- It generalizes readily to multiple dimensions.
- It enforces positivity if ρ^ℓ is positive and if the allowed extrema ρ^{\min} and ρ^{\max} are adequately constrained.
- It prevents the creation of new extrema and the enhancement of existing ones.
- However, *the creation of new and the enhancement of existing numerical ripples* in the solution ρ^n is allowed in multidimensional problems, *i.e.*, the limiter is not monotone.

To see that these last two statements are not in conflict, consider the quasi-one-dimensional discontinuity shown schematically in Fig. 2. Imposed on the steep portion of the profile is a transverse ripple which the high-order convection algorithm can create

initially or amplify from its current amplitude, *above and beyond what the convection and sources may produce physically*. Zalesak’s limiter does not prevent this from happening so long as the excursions associated with the ripple do not surpass the local extrema. These extrema are located ahead of and behind the ripple, along the direction of principal variation in the profile. The ripple shown may grow until its maximum or minimum value reaches those of the neighboring extrema.

5. A MONOTONE MULTIDIMENSIONAL LIMITER

Clearly, it is desirable that the transverse ripple in Fig. 2 not be amplified during the antidiffusion stage of the FCT solution, nor should it be created in the first place, unless the convection and sources conspire to produce it. This suggests that the limiter be extended to prevent the creation of new and the enhancement of existing *directional* extrema, *i.e.*, extrema with respect to each coordinate direction considered independently. The solution adopted here is to apply Boris and Book’s limiter along each coordinate direction separately, as a prelimiting step in the FCT procedure. Within the context of Zalesak’s limiter, this prelimiting step replaces and augments the sign-reversal step B. It is important to note that the remainder of Zalesak’s procedure must still be carried out. Antidiffusive fluxes acting in concert on cells that are not directional extrema of ρ^ℓ could conspire to produce new local maxima or minima in ρ^n .

The resulting limiter, here expressed for a two-dimensional problem for definiteness, consists of the following steps:

- A. Establish allowed extrema ρ^{\min} and ρ^{\max} in each cell,

$$\begin{aligned}\rho_{i,j}^{\min} &= \min(\rho_{i,j-1}^\ell, \rho_{i-1,j}^\ell, \rho_{i,j}^\ell, \rho_{i+1,j}^\ell, \rho_{i,j+1}^\ell), \\ \rho_{i,j}^{\max} &= \max(\rho_{i,j-1}^\ell, \rho_{i-1,j}^\ell, \rho_{i,j}^\ell, \rho_{i+1,j}^\ell, \rho_{i,j+1}^\ell).\end{aligned}\tag{10}$$

- B. Prelimit the antidiffusive fluxes along each coordinate direction, to prevent the creation and enhancement of directional extrema and to reverse any antidiffusive flux that is directed down the gradient of ρ^ℓ ,

$$F_{i+1/2,j}^{a'} = \sigma_{i+1/2,j} \max \left[0, \min \left(\left| F_{i+1/2,j}^a \right|, \sigma_{i+1/2,j} V_{i,j} \Delta \rho_{i-1/2,j}^\ell, \right. \right. \\ \left. \left. \sigma_{i+1/2,j} V_{i+1,j} \Delta \rho_{i+3/2,j}^\ell \right) \right],\tag{11}$$

$$F_{i,j+1/2}^{a'} = \sigma_{i,j+1/2} \max \left[0, \min \left(\left| F_{i,j+1/2}^a \right|, \sigma_{i,j+1/2} V_{i,j} \Delta \rho_{i,j-1/2}^\ell, \right. \right. \\ \left. \left. \sigma_{i,j+1/2} V_{i,j+1} \Delta \rho_{i,j+3/2}^\ell \right) \right]. \quad (12)$$

C. Compute the total incoming and outgoing antidiffusive fluxes F^{in} and F^{out} in each cell,

$$F_{i,j}^{\text{in}} = \max \left(F_{i-1/2,j}^{a'}, 0 \right) - \min \left(F_{i+1/2,j}^{a'}, 0 \right) \\ + \max \left(F_{i,j-1/2}^{a'}, 0 \right) - \min \left(F_{i,j+1/2}^{a'}, 0 \right), \\ F_{i,j}^{\text{out}} = \max \left(F_{i+1/2,j}^{a'}, 0 \right) - \min \left(F_{i-1/2,j}^{a'}, 0 \right) \\ + \max \left(F_{i,j+1/2}^{a'}, 0 \right) - \min \left(F_{i,j-1/2}^{a'}, 0 \right). \quad (13)$$

D. Determine the fractions of the incoming and outgoing fluxes that can be applied to each cell,

$$f_{i,j}^{\text{in}} = (\rho_{i,j}^{\text{max}} - \rho_{i,j}^\ell) V_{i,j} / F_{i,j}^{\text{in}}, \\ f_{i,j}^{\text{out}} = (\rho_{i,j}^\ell - \rho_{i,j}^{\text{min}}) V_{i,j} / F_{i,j}^{\text{out}}. \quad (14)$$

E. Limit each antidiffusive flux so that it creates neither an undershoot in the cell it is leaving nor an overshoot in the cell it is entering,

$$F_{i+1/2,j}^c = F_{i+1/2,j}^{a'} \times \begin{cases} \min (f_{i,j}^{\text{out}}, f_{i+1,j}^{\text{in}}, 1), & \text{if } F_{i+1/2,j}^{a'} \geq 0; \\ \min (f_{i,j}^{\text{in}}, f_{i+1,j}^{\text{out}}, 1), & \text{otherwise;} \end{cases} \\ F_{i,j+1/2}^c = F_{i,j+1/2}^{a'} \times \begin{cases} \min (f_{i,j}^{\text{out}}, f_{i,j+1}^{\text{in}}, 1), & \text{if } F_{i,j+1/2}^{a'} \geq 0; \\ \min (f_{i,j}^{\text{in}}, f_{i,j+1}^{\text{out}}, 1), & \text{otherwise.} \end{cases} \quad (15)$$

This procedure differs from Zalesak's original only in the crucially important prelimiting step B.

6. EXAMPLES

Two hydrodynamical problems will be used to illustrate the performance of the proposed multidimensional FCT flux limiter. The first is a two-dimensional, Cartesian muzzle-flash simulation. A 3.2 cm \times 3.2 cm section of the tube is represented by a 320 \times 320 grid of uniformly space cells. Vertically bisecting and extending 1.2 cm into the domain from the left edge is a solid divider whose thickness is .16 cm (120 \times 16 cells). A stoichiometric mixture of hydrogen and oxygen gas, whose molecular weight is 12 and ratio of specific

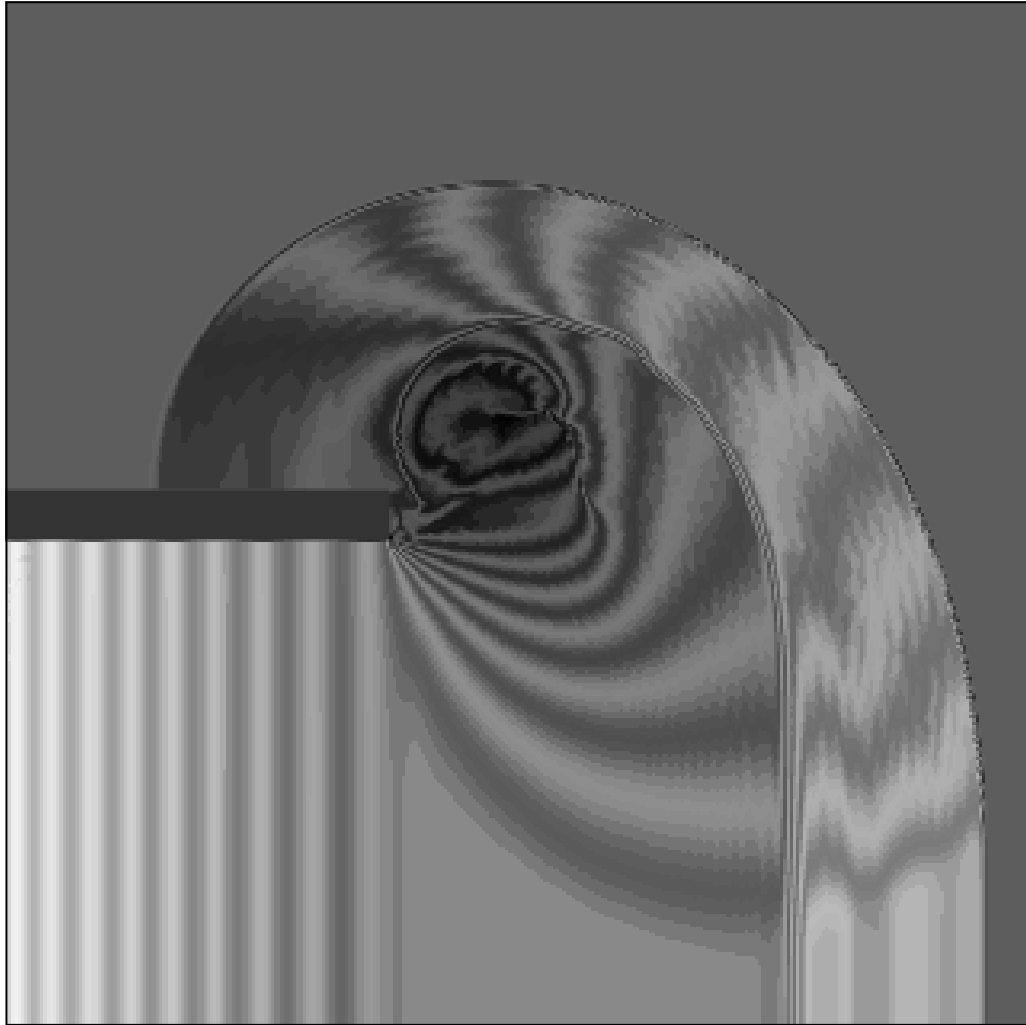


Fig. 3. Results of a Cartesian muzzle-flash simulation are shown at a fixed time after a diaphragm, extending from the end of the horizontal divider to the bottom of the domain, bursts. The mass density is shaded over its full range of variation (a factor of 5.5). Zalesak’s flux limiter was used. Note the prominent ripples at the edges of the light- and dark-shaded regions, behind the shock front.

heats is $7/5$, fills the tube. Behind a diaphragm extending from the end of the solid wall down to the bottom edge of the domain, the mixture is at a pressure of 20 atm and a temperature of 1000 K. Elsewhere the pressure and temperature are at standard conditions. The diaphragm bursts at time $t = 0$, allowing the hot, pressurized gas to flow into the chamber.

The Euler equations were solved using a two-dimensional FCT hydrodynamics scheme, *LCPFCT2*, described elsewhere (DeVore 1989). It is the 2D extension of Boris and Book’s one-dimensional, low phase error algorithm *LCPFCT* (Boris & Book 1976b; Boris *et al.* 1993), and shares with it fourth-order accuracy in phase and amplitude at long wavelengths.

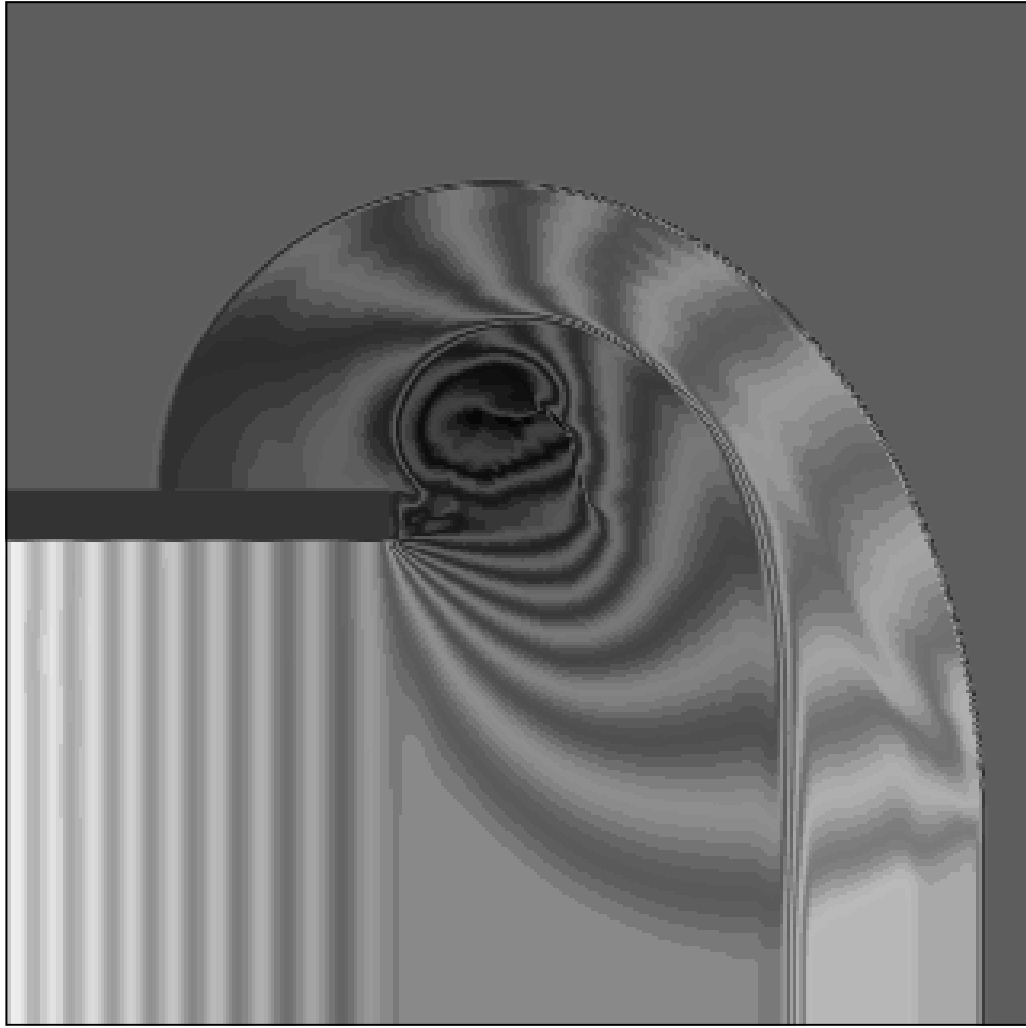


Fig. 4. Same as Fig. 3, but using the new monotone flux limiter. The prominent ripples evident in Fig. 3 are largely eliminated.

The boundaries were closed with reflecting conditions at the top and bottom of the domain and along the tube's divider, and open with zero-gradient conditions at the left and right edges of the domain. A Courant number of .25 was used.

Computed solutions for the mass density after an elapsed time of $15 \mu\text{s}$, using Zalesak's flux limiter and the proposed monotone limiter, are shown in Figs. 3 and 4, respectively. Along the bottom edge of the domain, the solution is approximately that of the one-dimensional Riemann problem. The outermost discontinuity in the density is the shock wave, propagating toward the right edge of the domain near the bottom. It is followed by the contact discontinuity, which is attached to the open end of the divider and reaches about 75% of the way across the domain at the bottom. A rarefaction wave propagates toward the left below the divider. The expansion of the fluid upward and to the left at the

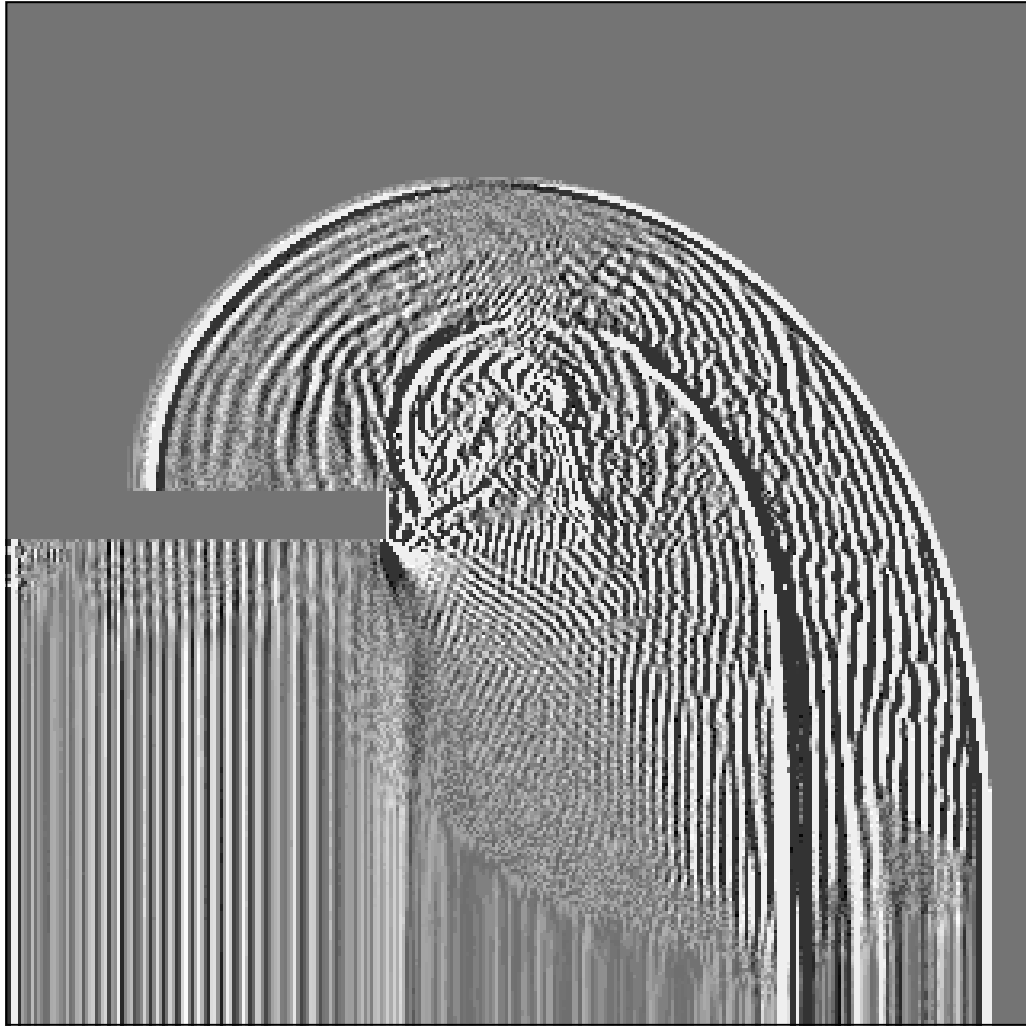


Fig. 5. Second derivatives along the horizontal coordinate of the mass densities obtained with Zalesak’s limiter and displayed in Fig. 3 are shown. The color table’s range is restricted to saturate the shock and contact surface and bring out the lower-amplitude, numerical fine structure. Note the rapid oscillations between maxima and minima behind both the shock front and the contact surface.

open end of the divider creates a vortex there. These principal features of the calculation are well defined in both cases. Zalesak’s limiter, however, also produces a substantial amount of oscillatory fine structure in its solution. This is evident as fingers emanating from the shaded bands, especially in the region between the shock wave and the contact surface. This fine structure is predominantly numerical in origin.

In order to bring out the spurious structure and highlight the differences between the two calculations, the second derivative of the mass density along the horizontal coordinate is displayed in Figs. 5 and 6 for Zalesak’s limiter and the new limiter, respectively. A low value for the extremal amplitudes spanned by the color table was selected, so that the shock

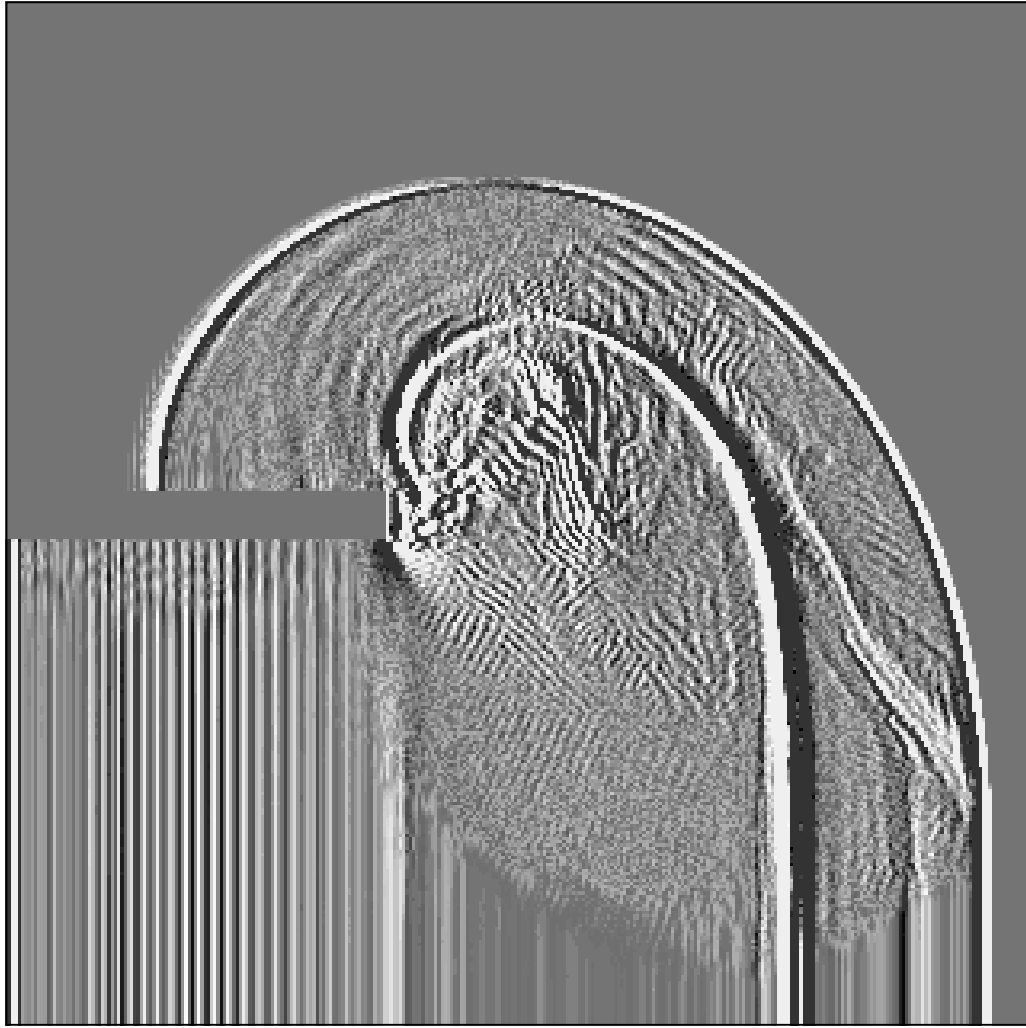


Fig. 6. Same as Fig. 5, but obtained from the density field in Fig. 4, which used the monotone flux limiter. The rapid oscillations clearly evident in Fig. 5 are greatly suppressed.

wave, contact surface, and edge of the divider strongly saturate the figures, allowing the smaller-amplitude fine structure to be brought out. Prominent striations fill much of the volume between the shock and contact surface and to a lesser extent the volume inside the contact surface, in the calculation using Zalesak's limiter. These features are much weaker through most of the domain when the new limiter is used, as can be seen by comparing Figs. 5 and 6. An exception is the small-amplitude density jump between the shock front and the contact surface that is evident in the right panel. This structure is faithfully reproduced in an operator-split integration of the Euler equations for this problem using *LCPFCT* (not shown). It apparently is an artifact of the initial conditions, developing in the early evolution of the system as the shock, contact surface, and rarefaction wave form and separate from their common origin (Boris & Oran 1995). Multiple such structures can

be seen in Fig. 5, near the bottom edge of the domain between the shock and the contact surface. These additional waves evidently are excited by the action of the non-monotone flux limiter.

The second example is a three-dimensional simulation of a subsonic rectangular jet (Grinstein 1995). An initially laminar air jet at standard temperature and pressure issues from a rectangular nozzle of aspect ratio 4:1 at Mach 0.6. The quiescent background gas also is at STP. In order to focus on the dynamics of the individual vortex rings of the jet, an isolated ring is puffed out by closing off the inflow boundary after a finite time equal to the ratio of the jet equivalent diameter to the flow speed. The evolution of the ring is then followed as it convects downstream.

The numerical model uses *LCPFCT2* to solve for the flows in the 2D cross-stream plane, and *LCPFCT* for the streamwise direction. A $150 \times 110 \times 110$ grid was used to represent the domain, with the cells evenly spaced in the shear-flow region of the jet and geometrically stretched in the cross-stream directions outside. The Courant number was 0.5. Fixed mass density and velocity conditions were specified on the boundary cells defining the jet orifice, with free-slip conditions obtaining elsewhere on the entrance plane. Advection conditions were imposed on those quantities at the outflow boundary, and all variables satisfy stagnation-flow conditions at the cross-stream boundaries. The pressure satisfies the inviscid 1D pressure equation at the jet orifice and a non-reflecting condition at the outflow boundary.

Time sequences of isosurfaces of the vorticity magnitude are shown in Figs. 7 and 8, obtained using Zalesak's limiter and the monotone limiter, respectively, in the 2D FCT module. In the figures, time increases from left to right and from bottom to top. The bottom-most six frames in each figure show the self-induced deformation and axis switching of the vortex ring. The highly curved corners accelerate ahead of the ring sides and toward the centerline, pulling the minor axis sides along with them. This process bends the ring along its major axis. The increasing curvature at the midpoints of the major sides accelerates those portions streamwise toward the leading minor sides but away from the jet centerline. This results in a nearly planar, axis-switched configuration of the vortex ring at frame 6. This early evolution is essentially identical in the two cases, save for some intermittent, small-scale, numerical features evident with Zalesak's limiter.

Subsequently, the ring's new major sides pinch together and reconnect, forming a pair of vortex rings linked on the underside by two thin threads. This is shown in the

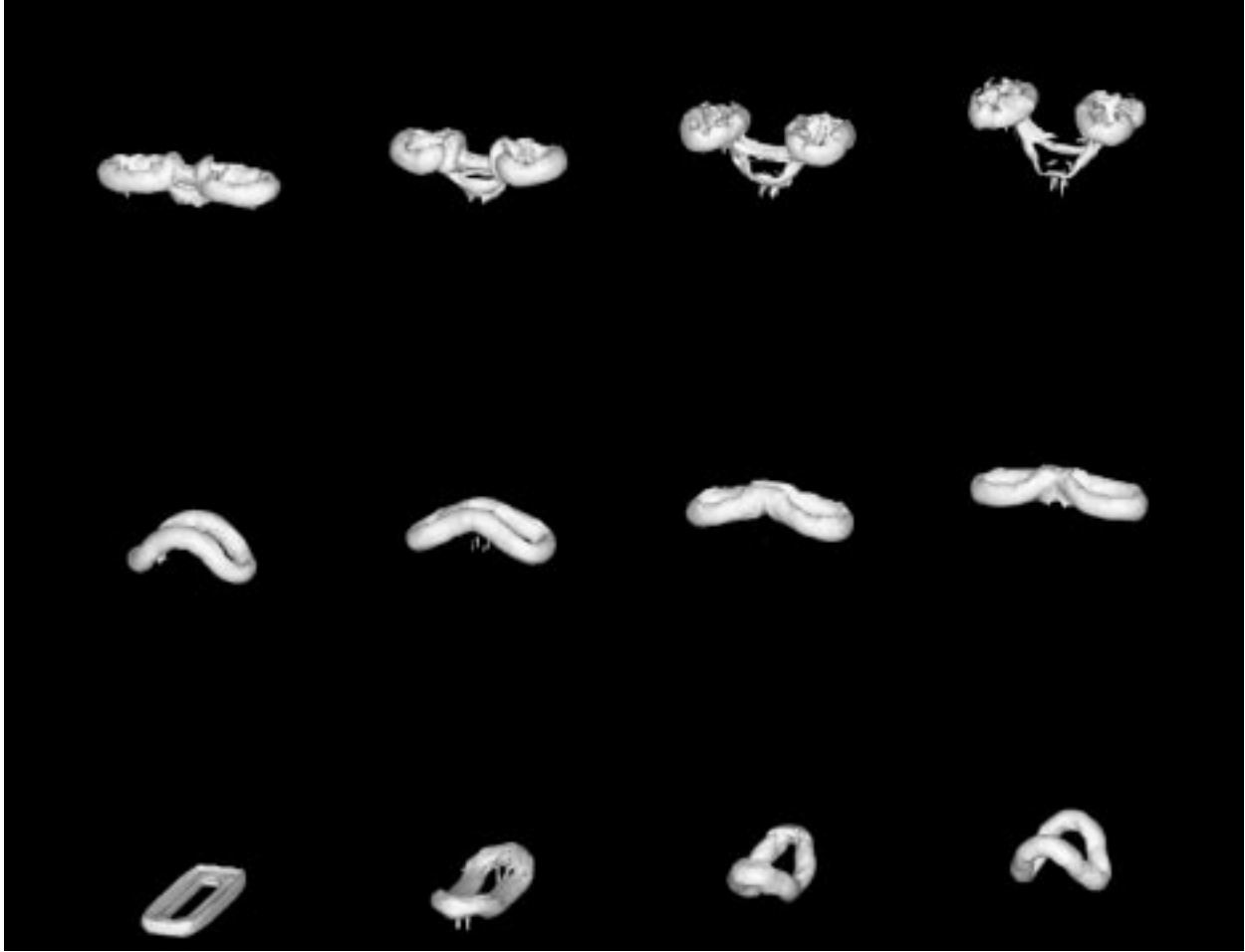


Fig. 7. Self-deformation, reconnection, and subsequent merging of an isolated vortex ring are shown. The ring is puffed from a Mach 0.6 air jet whose aspect ratio is 4:1. Isosurfaces of the vorticity magnitude are shown at 15% of the peak initial vorticity. Time increases from left to right and from bottom to top in the figure. These results were obtained using Zalesak’s flux limiter.

following six panels of Figs. 7 and 8. While both simulations clearly show the bifurcation of the ring, the fine structure associated with the threads bridging the two daughter rings increasingly differs between the two limiters. Zalesak’s limiter permits fluctuations on the threads of vorticity, which show up as spikes attached to the isosurfaces and lead at frame 12 to the fragmenting of the threads. Note that the two daughter vortex rings appear to be irrevocably separating. In contrast, with the new limiter the fine structure is cleanly and clearly represented through frame 12, the vorticity threads remain intact, and the daughter rings stay in close proximity to one another. Indeed, as the assembly proceeds further downstream, the vortex rings’ outer edges accelerate ahead while their inner edges migrate towards the centerline, merge, and reconnect. This is shown in the top four panels of Fig. 8, and in even later images in Grinstein (1995). Features at still smaller

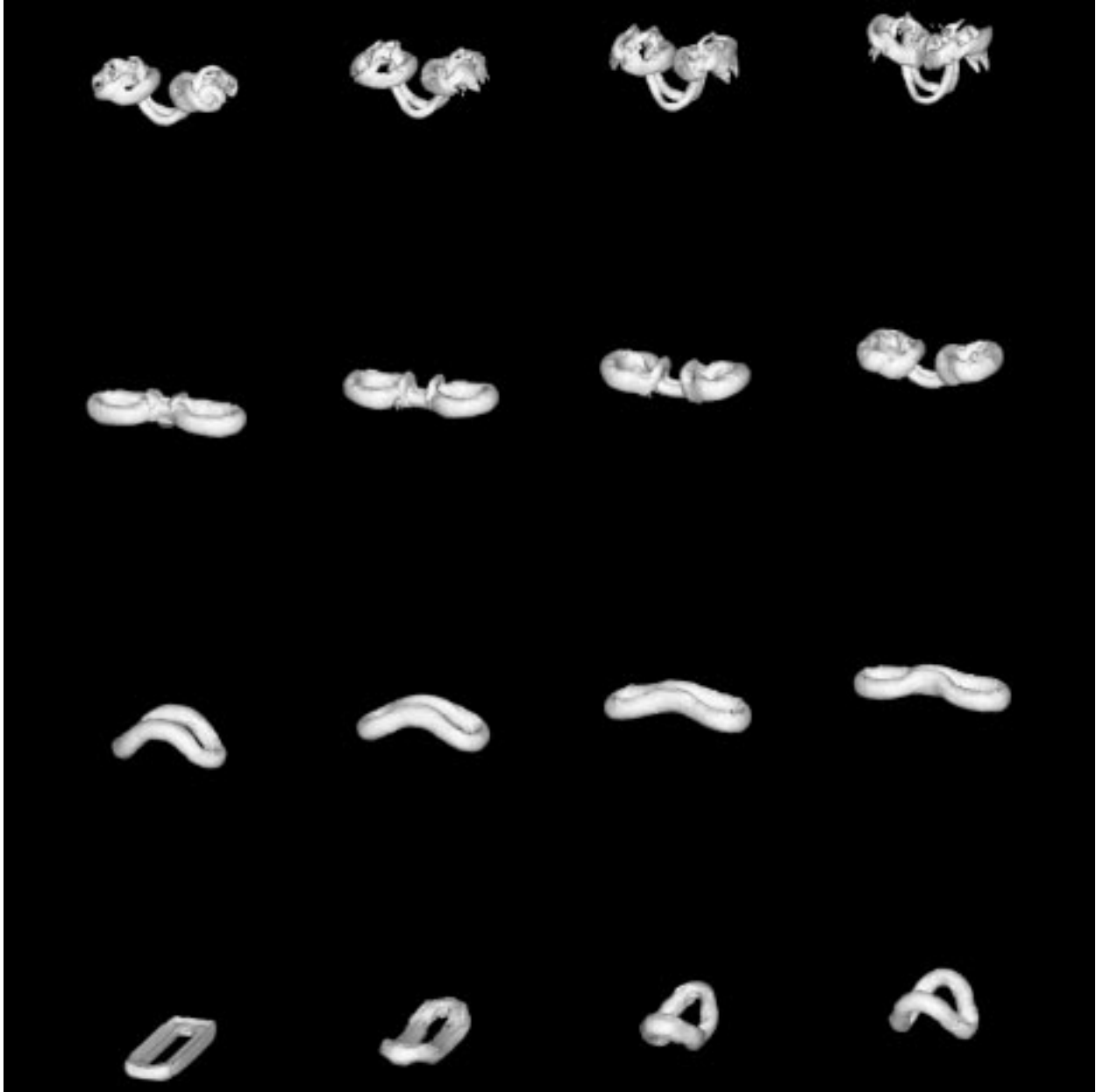


Fig. 8. Vortex ring evolution depicted in Fig. 7, but here calculated with the montone flux limiter. The lower twelve frames coincide precisely in time with the frames of the preceding figure.

scales than before, within the vortex rings themselves, become visible and can be tracked readily during this phase of the evolution. This example dramatically demonstrates that the dynamical behavior of the system, above and beyond the aesthetics of the simulation results, can be influenced significantly by the choice of flux limiter.

7. DISCUSSION

An improved prescription for limiting the fluxes in multidimensional, flux-corrected transport calculations has been proposed. This modification to Zalesak's (1979) original multidimensional limiter is motivated by the observation of numerical ripples of modest amplitude in two- and three-dimensional FCT solutions of hydrodynamical and MHD systems. The occurrence of such ripples is traced to the absence of a monotonicity constraint in Zalesak's limiter, which nevertheless is positivity preserving and prohibits the creation of new and the enhancement of existing extrema. The recommended modification is the addition of a prelimiting step which imposes the same prohibition on directional extrema, *i.e.*, any maxima and minima of the transported quantity when considered along each coordinate direction independently. This is accomplished by applying Boris and Book's (1973) original, one-dimensional flux limiter to the unidirectional antidiffusive fluxes.

Two numerical examples shown illustrate the prevalence of small-scale, relatively low-amplitude fluctuations in solutions obtained with Zalesak's limiter, due to the lack of a monotonicity constraint. These fluctuations are very effectively suppressed by the new limiter, leading to obvious aesthetic improvements in the FCT solutions. More importantly, the rectangular jet simulation demonstrates compellingly that qualitative changes in the system's dynamical evolution can ensue from the improved representation of its small-scale structures.

Some final remarks are offered concerning one other facet of Zalesak's FCT limiter: the flexibility available in establishing the allowed extrema in each computational cell (step A of the limiting procedure). In order to counter FCT's tendency to 'clip' the maxima and minima of a transported quantity and form three-cell-wide extrema, Zalesak suggested looking back to the starting values at each timestep, or even linearly extrapolating to find extrema between cells, in addition to considering the positive and monotone provisional solution to which the corrected antidiffusive fluxes are added. This generalization seems to be advantageous in linear advection problems, where the velocity is fully specified and minimizing the residual numerical diffusion is desirable. In solutions of nonlinear systems such as the Euler equations of hydrodynamics, on the other hand, this increased flexibility in the limiter tends to create more numerical ripples of greater amplitude. Fluctuations in the pressure, *e.g.*, create associated fluctuations in the velocities, and the resulting feedback loops are detrimental to the smoothness of the solutions obtained. Restricting

the determination of the allowed extrema to the neighboring provisional values along the coordinate axes provides sufficiently accurate, but also monotone, solutions.

ACKNOWLEDGEMENTS

Acknowledgements are due Jay P. Boris, David L. Book, Steven T. Zalesak, John H. Gardner, and Gopal Patnaik for many helpful discussions on the foundations and extensions of FCT techniques, and Elaine S. Oran, Fernando F. Grinstein, Judith T. Karpen, Spiro K. Antiochos, and Nicholas A. Tonello for sharing experiences in applying these methods to a variety of problems. This work was supported by the National Aeronautics and Space Administration's High Performance Computing and Communications program for Earth and Space Sciences and by the Office of Naval Research through the Naval Research Laboratory.

REFERENCES

- Antiochos, S. K. and C. R. DeVore, "The role of magnetic reconnection in solar activity," in *Physics of Sun-Earth Plasma and Field Processes*, edited by J. L. Burch, R. L. Carovillano and S. K. Antiochos (American Geophysical Union, Washington, 1999a), in press.
- Antiochos, S. K. and C. R. DeVore, "The role of helicity in magnetic reconnection: 3D numerical simulations," in *Magnetic Helicity in Space and Laboratory Plasmas*, edited by R. C. Canfield and A. A. Pevtsov (American Geophysical Union, Washington, 1999b), in press.
- Antiochos, S. K., C. R. DeVore and J. A. Klimchuk, "A model for solar coronal mass ejections," *Astrophys. J.* (1999), in press.
- Book, D. L., J. P. Boris and K. Hain, "Flux-corrected transport, II: Generalizations of the method," *J. Comput. Phys.* **18**, 248 (1975).
- Boris, J. P. and D. L. Book, "Flux-corrected transport, I: SHASTA, a fluid transport algorithm that works," *J. Comput. Phys.* **11**, 38 (1973).
- Boris, J. P. and D. L. Book, "Flux-corrected transport, III: Minimal-error FCT algorithms," *J. Comput. Phys.* **20**, 397 (1976a).
- Boris, J. P. and D. L. Book, "Solution of continuity equations by the method of flux-corrected transport," in *Methods of Computational Physics* (Academic Press, New York, 1976b), p. 85.

- Boris, J. P., A. M. Landsberg, E. S. Oran and J. H. Gardner, "LCPFCT - A flux-corrected transport algorithm for solving generalized continuity equations," Naval Research Laboratory Report No. 6410-93-7192, 1993.
- Boris, J. P. and E. S. Oran, personal communication (1995).
- DeVore, C. R., "Flux-corrected transport algorithms for two-dimensional compressible magnetohydrodynamics," Naval Research Laboratory Report No. 6544, 1989.
- DeVore, C. R., "Flux-corrected transport techniques for multidimensional compressible magnetohydrodynamics," *J. Comput. Phys.* **92**, 142 (1991).
- Grinstein, F. F., "Self-induced vortex ring dynamics in subsonic rectangular jets," *Phys. Fluids* **7**, 2519 (1995).
- Grinstein, F. F. and C. R. DeVore, "Dynamics of coherent structures and transition to turbulence in free square jets," *Phys. Fluids* **8**, 1237 (1996).
- Karpen, J. T., S. K. Antiochos and C. R. DeVore, "On the formation of current sheets in the solar corona," *Astrophys. J.* **356**, L67 (1990).
- Karpen, J. T., S. K. Antiochos and C. R. DeVore, "Coronal current-sheet formation: The effect of asymmetric and symmetric shears," *Astrophys. J.* **382**, 327 (1991).
- Karpen, J. T., S. K. Antiochos and C. R. DeVore, "The role of magnetic reconnection in chromospheric eruptions," *Astrophys. J.* **450**, 422 (1994).
- Karpen, J. T., S. K. Antiochos and C. R. DeVore, "Reconnection-driven current filamentation in solar arcades," *Astrophys. J.* **460**, L73 (1996).
- Karpen, J. T., S. K. Antiochos, C. R. DeVore and L. Golub, "Dynamic responses to magnetic reconnection in solar arcades," *Astrophys. J.* **495**, 491 (1998).
- Oran, E. S. and J. P. Boris, *Numerical Simulation of Reactive Flow* (Elsevier, New York, 1987).
- Oran, E. S. and C. R. DeVore, "The stability of imploding detonations: Results of numerical simulations," *Phys. Fluids* **6**, 369 (1994).
- Tonello, N. A. and E. S. Oran, personal communication (1995).
- Zalesak, S. T., "Fully multidimensional flux-corrected transport algorithms for fluids," *J. Comput. Phys.* **31**, 335 (1979).